Hydrogen Bonding in Thioether Self-Assembly

A Senior Thesis for the Department of Chemistry

Allister McGuire

Committee: Dr. Elena Rybak-Akimova and Dr. Charles Sykes

April 27th, 2012

Tufts University, 2012

Introduction.

In recent experimental history, there is perhaps no more powerful surface-sensitive technique which has been developed from the ground, up as scanning tunneling microscopy (STM). Gerd Binnig and Heinrich Roher invented the scanning tunneling microscope and were awarded the 1986 Nobel Prize in physics for their work.[1] The instrument utilizes a phenomenon called "quantum tunneling" to achieve resolution on the order of nanometers in the x- and y-dimensions, and picometers in the z-dimension. Quantum tunneling derives its physical basis in quantum mechanics wherein the wave equations of a sufficiently light and small particle may penetrate the vacuum barrier between its current location and destination which would classically prevent its travel (Figure 1).

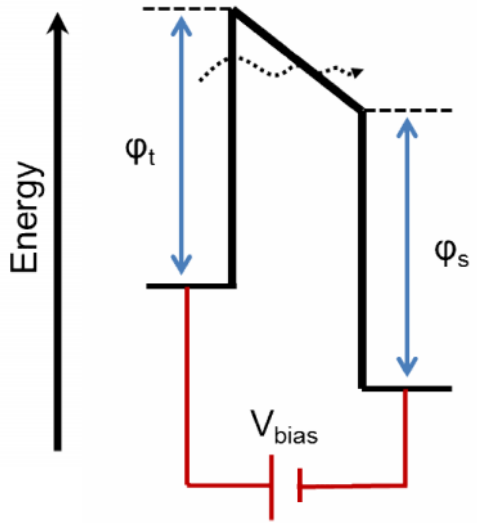

Figure 1. Schematic of quantum tunneling in STM. φ_t represents the work function of the conductive tip, φ_s represents the work function of the substrate and V_{bias} is the voltage applied between these two materials. When a positive bias is applied to the sample, for example, φ_s reduces, allowing more facile tunneling of electrons (represented by the dotted arrow) through the intervening barrier.

In STM, an electron tunnels between a conductive electrode "tip" (Figure 2) and a conductive substrate due to the presence of a bias applied to the substrate. This movement of

electrons generates a small but measureable current which is exponentially related to the distance between the tip and substrate by the equation:[2]

$$I \propto \frac{V_{bias}}{d} e^{-A\varphi^{1/2}d}$$

where I is the tunneling current, V_{bias} is the applied voltage, d is the distance between the tip and the sample, A is a constant that depends on the intervening barrier (vacuum or otherwise), and φ is the average of the tip and substrate work functions. This equation conveys the fact that STM gathers a convolution of topographical and electronic information from the measured system. Corrugation of the surface gives rise to a modulated current as does the presence of more- or less-conductive moieties between the tip and substrate (e.g. a hydrocarbon molecule).

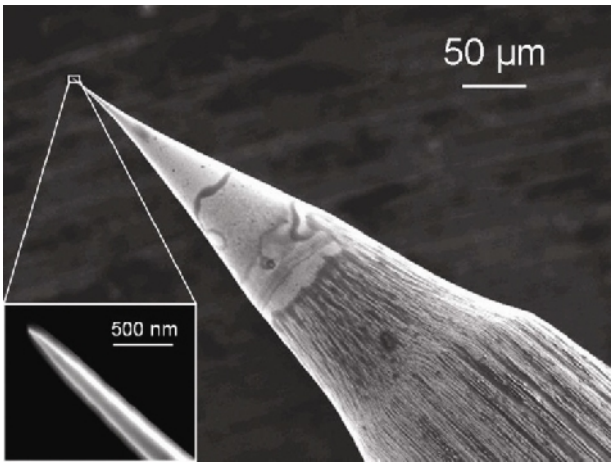

Figure 2. SEM image of a chemically etched tungsten metal tip. Despite the apparent sharpness of this tip, mutiple atoms could could share the end, convoluting the tunneling signal. To combat such effects, further tip conditioning is performed *in situ*.

Furthermore, STM is useful as the experimenter can tune the voltage of the tunneling electrons and thus the electrical field to which the measured system is exposed. When the measured system involves molecules, the tunneling electrons can cause excitation of these

molecules from their ground state to the precise excitation energy availed by the electrons' voltage. In this way, STM can probe the various molecular orbitals, energetic barriers, and charge states characteristic of the molecules.[3-5] Truly, this technique is most unique and powerful for its critically localized control over electron mobility both due to the proximity of the tip to the substrate/measured system as well as the exponential decay in tunneling probability as distance between the tip and conductive entity increases. This localization can also be used in single-molecule manipulation by decreasing the tip-to-sample distance, allowing electrostatic interactions and van der Waals forces to gently drag molecules across the surface.[6] Such a capacity allows one to probe the strength of molecule-surface interactions as well as to uncover interesting quantum phenomena such as the quantum corral.[7] Furthermore, tuning of electron energies against the resonant energy of a chemical bond can yield a variety of reactions, the first of which was a fully STM-instigated Ullmann reaction wherein two aryl halides were coupled at a Cu(111) step edge to form a covalently bonded diaryl species.[8]

A wide variety of experimental parameters can be manipulated in these experiments, for example, the mode of scanning. In constant current mode, a current is set by the experimenter and, as the tip rasters across the substrate, it adjusts the tip-substrate separation to maintain the assigned current. This is opposed to constant height mode in which the tip-sample separation is specified and, as the current modulates, an image is recorded. The second technique would afford a higher raster speed but would not be useful in a previously-uncharacterized system as small corrugation in the surface could induce crashing of the tip. Depending on one's familiarity with the system, there are tens or hundreds of like parameters that can be adjusted in the experimental setup.

The major shortcoming of STM is the fact that this microscopy cannot report chemical information. Therefore, a vacuum chamber is often used in order to minimize the opportunity for the system to be contaminated. A secondary method must be implemented to spectroscopically interrogate the system. Some spectroscopic methods utilize the STM components themselves, but augment the electronics in order to retrieve spectroscopic information. Others are separate spectroscopies which probe either the surface or first few layers of the surface by irradiating it with certain species—ions, atoms, photons, electrons, etc.—and characterizing their interaction with the sample via measurement at a specific detector.[9]

Ultra-high vacuum STM research is often conducted on single-facet crystals which have been precisely cut for this research. Single-facet crystals or "single crystals" allow for the study of highly fundamental intermolecular molecule-surface interactions, as one need not account for contribution across many different facets and conclusions may be made about intermolecular forces free of convolution with multiple surface geometries. The (111) facet is utilized in many common-metal surface studies because it is the most energetically stable facet in many cases, leading to its predominance on the surface of real (non-ideal) nanoparticles. Thus studies on hexagonally symmetric single crystals may be approximately informative to real system behavior, informing the design of practically useful materials.

One subset of these practically useful materials is those formed by self-assembly. Self-assembly is a phenomenon characteristic of some materials wherein any of a variety of intermolecular forces drives the ordered arrangement of molecules without the application of external driving forces. These intermolecular driving forces include van der Waals and electrostatic forces (e.g. hydrogen bonding). The most common example of self-assembly is solution based: the lipid bilayer (Figure 3).

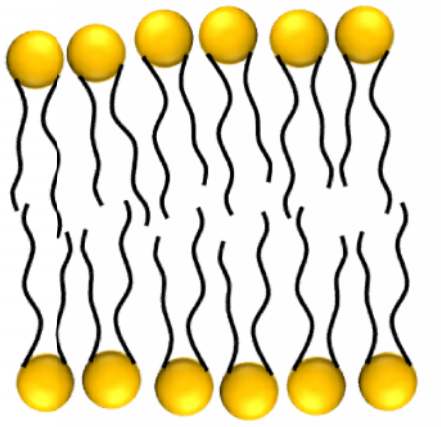

Figure 3. Schematic representation of the phospholipid bilayer. Yellow "head groups" represent charged phosphates while black "tails" represent nonpolar lipid chains.

The lipid bilayer composes the plasma membrane of most living cells and is extensively studied for application in drug delivery and biosensing.[10,11] Its *in vivo* formation is driven by both electrostatics between the phosphate head groups and polar solvent molecules (e.g. water) presented in aqueous interstitial fluid as well as van der Waals forces which favor aggregation of the bilayer's non-polar lipid tails.[12] It is this material that facilitates the diffusion of vital molecules into the cells, and prevents the entrance of foreign moieties, maintaining a precise homeostasis. As such, self-assembly is a critical process to organisms' livelihood.

Self-assembly is also prominent in the field of surface science due to the fact that a symmetric lattice provides an exceptional template on which organic molecules may assemble. There are a variety of applications for surface-bound organic films including supercapacitors, unobtrusive sensors, heterogeneous catalysts and microelectronics.[13-26] Much of the fundamental research in these fields has investigated the applicability of thiols. Thiols (RSH) have been shown to chemisorb to the gold substrate via proton dissociation yielding a thiolate-gold bond, as well as orient nearly perpendicularly to the surface.[27] They are preferred for many applications

because they are easily functionalized and because, by adjusting the length of the alkyl tail attached to the anchoring S atom, one can precisely tune the thickness of the film of interest. Therefore, thiols present a facile opportunity to functionalize a surface with a multiplicity of chemical and structural properties. However, there are also a variety of drawbacks involved with using thiol films. The films are susceptible to structural defects such as etch pits and rotational domain boundaries, which make the monolayers more susceptible to oxidation and displacement.[17,21,28-30] They also forfeit control over the lateral spacing of the molecules, i.e. one cannot tune the density of a full-monolayer thiol system. In contrast, thioethers (RSR') provide an answer to many of these shortcomings. Due to a weaker surface interaction, etch pits do not form, leading to greater uniformity across the surface and less opportunity for oxidation. Additionally, because these molecules adsorb molecularly, they have both tails intact when bound to the surface. Alkyl tails specifically have been shown to orient parallel to the surface, thus imparting control over the lateral spacing of the molecules at monolayer coverage.[31] These molecules are also easily functionalized and, to date, only a few studies have been conducted on sulfides of varying alkyl tail length and symmetry. [32-41]

Gold is often used in self-assembled systems for its strong interactions with the molecules under study. Sulfur-containing compounds are especially robust when adsorbed to Au, as series of thermal desorption experiments revealed, demonstrating that thiols adsorb with a binding energy of > 120 kJ/mol (1.3 eV) and while sulfides exhibited a binding energy of > 50 kJ/mol (0.57 eV).[42] From an experimental perspective, such a strong interaction may ensure that various microscopies and spectroscopies will not decompose the system, but it also makes a case for the generalizability of the results obtained—if the system were unstable on Au at low

temperature and pressure, there would be little hope for its stability at less ideal conditions. Thioethers and thiols alike can withstand ambient conditions, in and out of solution.[43]

Thioethers, then, represent an interesting alternative to alkane thiols as monomers for molecular self-assembly on metal surfaces. In a step towards designing thioether monolayers with multiple functionalities, we have investigated the molecular-scale assembly of 3-(methylthio)propanol (MTP), $CH_3SCH_2CH_2CH_2OH$, on Au(111) (Figure 4).

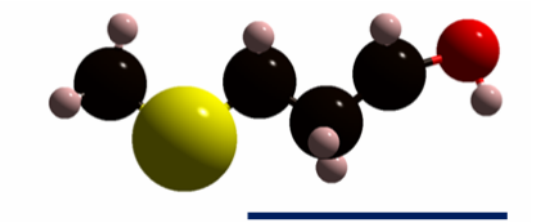

Figure 4. Molecular model of MTP. S is yellow, C is black, H is white, and O is red. Scale bar = 0.5 nm.

Scanning tunneling microscopy reveals that the hydroxyl groups at the C3 position drive the formation of an array of novel structures that are not observed with the analogous thioether, butyl methyl sulfide (BMS). The hydrogen-bonding-driven ordering yields linear chains and chiral hexamer rings that are very similar in structure to methanol assemblies on Au(111). At near-monolayer coverage, very ordered monolayers are observed. The adsorption is strong enough to lift the native herringbone reconstruction of the Au(111) surface but stops short of removing additional atoms, as is the case with thiols. While these monolayer structures are similar to those of the non-functionalized BMS, hydrogen bonding between adjacent rows leads to lamellar structures with a hydrophilic core and hydrophobic exterior. As such, these assemblies are one-dimensional analogues of the lipid bilayer.

Experimental.

All data were acquired in ultra-high vacuum conditions with low-temperature scanning tunneling microscope (STM) manufactured by Omicron NanoTechnology and operated at 5 or 78 K, as indicated. Chemically etched tungsten tips were used to probe the system. The Au(111) crystal (MaTecK) was cleaned prior to experiments by a series of Ar ion sputtering (1.0 keV) and annealing (1000 K) cycles. The sample was then transferred under ultra-high vacuum ($\sim 10^{-9}$ mbar) to the pre-cooled STM stage, and reached 5 or 78 K within 60 min. MTP (~98 %, Sigma Aldrich), BMS (~98 %, Sigma Aldrich), and methanol (99.8+%, Alfa Aesar) were further purified by *in situ* freeze/pump/thaw cycles. The analytes were then deposited onto the cold metal sample via a line-of-site collimated molecular doser. All voltages refer to the sample bias. One monolayer (ML) refers to the highest coverage ordered structure of each molecule with unit cells: c(7 x √3) for MTP, (√13 x √3) R13.9^{o} for BMS, and (11 x √3) for methanol. Annealing treatments were performed by transferring the sample to a room temperature holder inside the vacuum chamber for a pre-determined period of time to reach the desired temperature, and annealing temperatures are reported within 20 K accuracy. All anneal treatments are judged according to the transfer time; this transfer time is then correlated to an effective temperature which was standardized in dimethyl sulfide diffusion experiments.[41] Au herringbone separations were measured from large scale images and represent the average separation perpendicular to the $[11\bar{2}]$ surface lattice direction (i.e. parallel to the close-packed direction).

Results and Discussion.

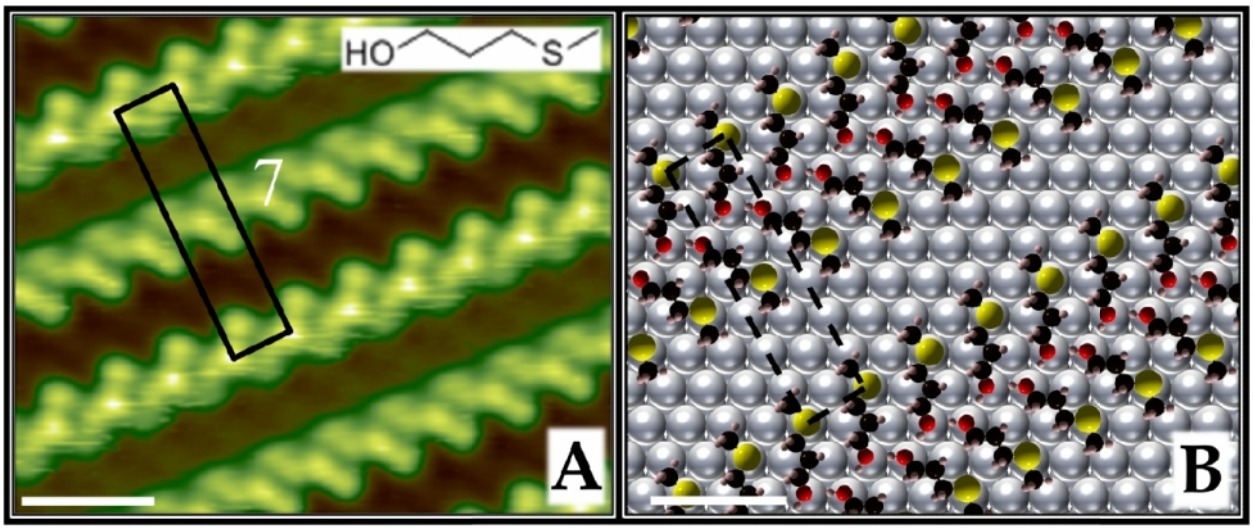

Figure 5. (A) STM image of MTP at near-monolayer coverage on Au(111). The black rectangle represents the common unit cell—c(7 x √3). The inset shows the chemical structure of MTP. (B) Schematic representation of the c(7 x √3) unit cell. The light grey sphere represents Au, S is yellow, C is black, H is white, and O is red. Scale bars show 1 nm. Imaging conditions for A: I_t = *300 pA,* V_s = *100 mV, T = 5 K.*

The ordering of MTP was studied as a function of coverage and annealing temperature (120 - 300 K). Annealing the sample ensured that the assemblies examined were equilibrium structures and not metastable arrangements.[44] Deposition of > 1 ML of MTP on Au(111) followed by annealing to 120 K resulted in the formation of large-scale self-assembled arrays with a periodic geometry as shown in Figure 5A. The molecules appear to order in regular paired rows; Figure 5B shows a schematic for the proposed molecular arrangement. In addition to weak dispersion interactions with the surface, the adsorption geometry of MTP is dictated by its two anchoring groups—a thioether sulfur atom and a primary hydroxyl—which are connected via the trimethylene backbone. Density functional theory (DFT) calculations have shown that thioethers adsorb on Au(111) via a dative S-Au bond and maintain tetrahedral geometry around the S atom.[45,46] Due to the additional O-Au interaction, adsorbed MTP has one less degree of freedom than its non-functionalized analogue, BMS. A back-of-the-envelope calculation suggests that, in

the gas phase, MTP has an O-S separation of 0.52 nm,[47] which agrees well with the C4-S spacing for BMS.[46] DFT calculations have shown that thioethers adsorb to Au with their S atoms at near atop sites;[31,33] it has further been shown that methanol also binds with its O atom atop.[48] The Au(111) atomic spacing in the $[11\bar{2}]$ ("√3") and equivalent directions is ~0.5 nm ($\sqrt{3}d_{Au}$); thus Au lattice offers the ideal surface geometry to accommodate bidentate adsorption of MTP with its flexible trimethylene backbone, as shown in Figure 5B. As there are three equivalent $[11\bar{2}]$ directions, MTP assembles along three directions on the Au surface. This monolayer structure sets neighboring molecules such that both O-O and S-S distances are separated by 0.5 nm, which agrees well with spacings previously observed on Au for thioethers and hydrogen bonded networks in which the O atoms sit at adjacent atop sites and the network zig-zags along the $[11\bar{2}]$ direction. At high coverages, single domains often span areas of the surface greater than 2,000 nm^2.

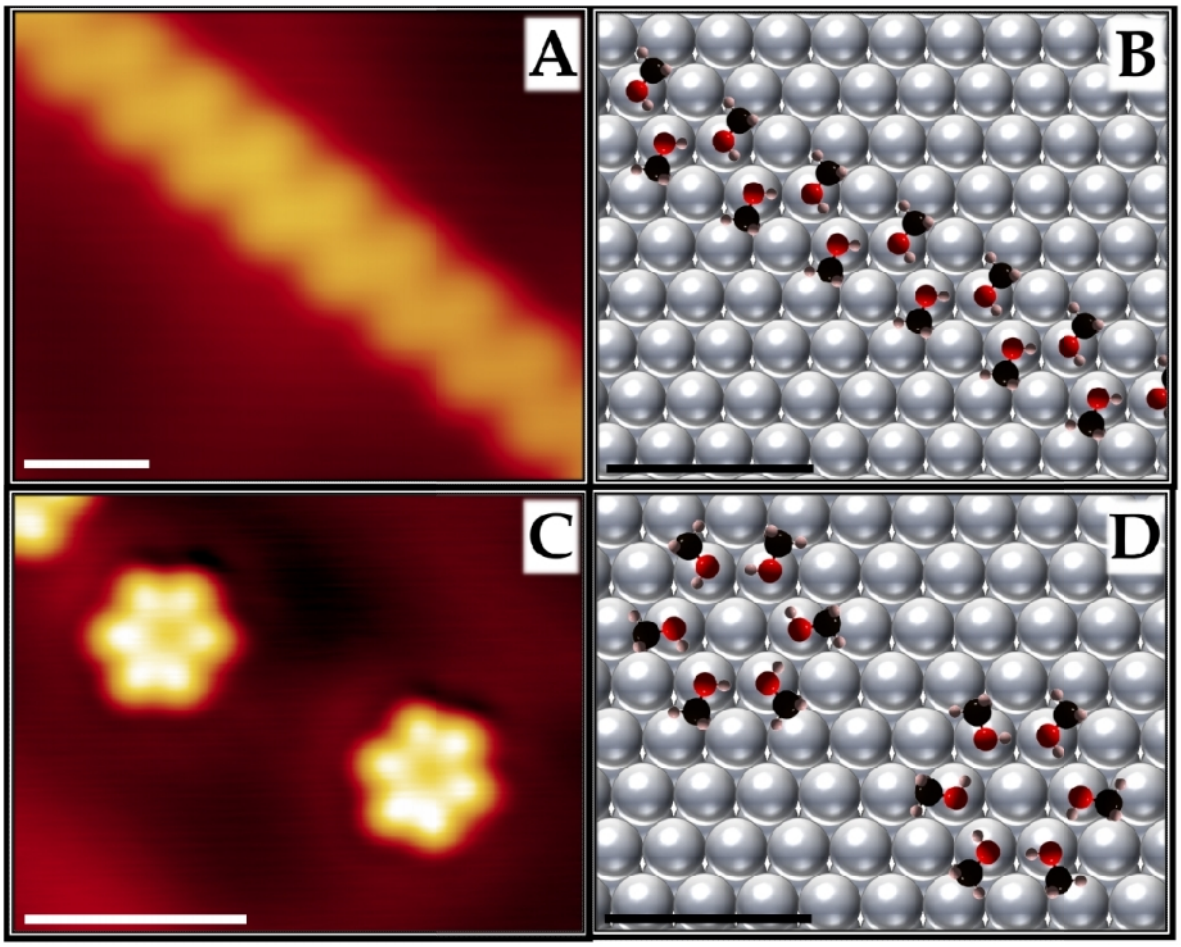

Figure 6. (A) STM image of a self-assembled methanol chain on Au(111). Imaging conditions: I_t = *50 pA,* V_s = *-100 mV, T = 5 K.* (B) Schematic of methanol's surface adsorption geometry dictated by a zig-zag hydrogen bonded network. (C) STM image of chiral methanol hexamer units on Au(111). Chirality arises by virtue of the hydrogen bond directionality that leads to a slight rotation of the clusters relative to one another. Imaging conditions: I_t = *30 pA,* V_s = *-100 mV, T = 5 K.* (D) Schematic of the hexamer structures. All scale bars indicate 1 nm.

In order to understand the ideal geometry of hydrogen bonded networks in MTP self-assembly, it is useful to evoke the preferred arrangements of a simpler molecule, methanol, on Au(111). At higher coverage, methanol forms chains on Au(111) directed by intermolecular hydrogen bonding (Figures 6A and 6B).[49] These chains lie along the and equivalent directions on Au(111) with the O atoms adsorbed at near atop surface sites. At low coverage, methanol forms discrete hexamers as shown in Figure 6B; these hexamers are chiral by virtue of

the direction of their hydrogen bonded network.[48] We found via STM and DFT that the hexamers with a clockwise O-H···O-H hydrogen bonded network were rotated clockwise from Au's close-packed direction, and those with an anti-clockwise H bonded network were rotated anti-clockwise from the close-packed lattice direction rendering the two hexamer forms as mirror image enantiomers of one another. Importantly, the O-O spacing in both hexamers and chains (0.27) is in agreement with the ideal hydrogen bond distance in liquid methanol's hydrogen bonded networks (0.29 nm).[50] Au's atomic lattice spacing is 0.288 nm, which coincides well with that of a hydrogen bond, thus supporting the proposed molecular arrangement for MTP in Figure 5B, in which a single Au atom separates O atoms on neighboring MTP molecules. Along a single row within the MTP monolayer, the O-O distance was measured to be 0.49 ± 0.07 nm using high-resolution STM images as shown in Figure 5, which is consistent with the $\sqrt{3}$ spacing in the zig-zag chains. MTP chains are therefore akin to methanol chains in that they run in the $[11\bar{2}]$ directions at full monolayer coverage (Figure 7).

Two rows of molecules connected by a hydrogen bonded backbone constitute a 'chain'. In STM images, these chains appear with the interior hydrogen bonded network imaging as a depression, while the remainder of the molecule images as a protrusion. The base unit in a chain is composed of two adjacent MTP molecules participating in hydrogen bonding. At monolayer coverage, MTP forms a lamellar overlayer composed of highly ordered parallel chains. This observed lamellar structure exhibits what Zhang, *et al.* have titled "herringbone-like packing" wherein the long axis of each molecule composing a base unit is not parallel to its counterpart, but instead the pair make an obtuse angle, measured here as 107 ± 3°.[51] Additionally, each MTP chain resembles a methanol chain with a hydrophilic core and a hydrophobic exterior.[49] The system, therefore, has the same basic structure of the methanol monolayer network on Au(111)

but is much more robust due to strong S-Au bonding and additional van der Waal's interactions both between molecules and with the surface. This is evidenced by MTP desorption at > 300 K vs. 155 K for methanol on Au(111).[52]

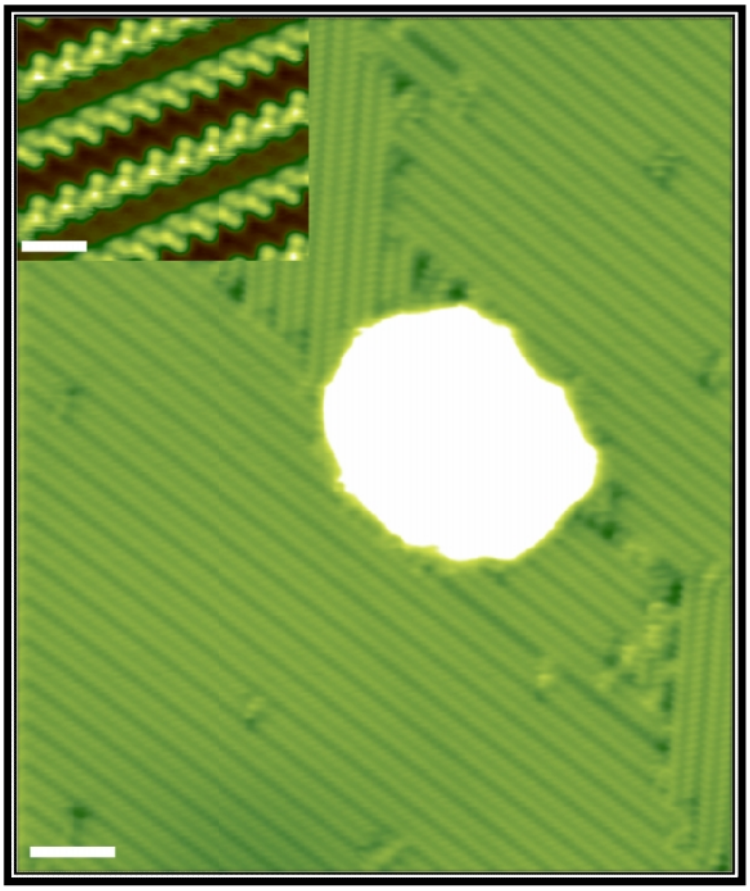

Figure 7. Long-range ordering seen in a 42 nm x 50 nm STM image of the near-monolayer MTP/Au system. The center feature is a gold island washed out due to image contrasting. Scale bar = 5 nm. Imaging conditions: I_t = *100 pA,* V_s = *100 mV, T = 5 K.* Inset shows high-resolution detail of lamellar rows. Scale bar = 1 nm. Imaging conditions: I_t = *300 pA,* V_s = *100 mV, T = 5 K.*

The lamellar structure resulting from hydrogen bonding between MTP molecules is distinct from that observed for BMS, which instead forms domains of rows in which all the butyl groups point one way as shown in Figure 8B.[39] In a space filling sense MTP is almost identical

to BMS.[39,46] Because of its increased symmetry, BMS on Au(111) has a compact (√13 x √3) R13.9° unit cell (Figure 4), while MTP predominantly shows a c(7 x √3) unit cell due to the pairing of adjacent MTP rows. In both BMS and MTP, however, the molecular packing densities (molecules/nm^2) are the same. These results indicate that MTP monolayers provide an opportunity for added functionality while retaining both the structural motifs and packing density expected for non-functionalized thioether overlayers.

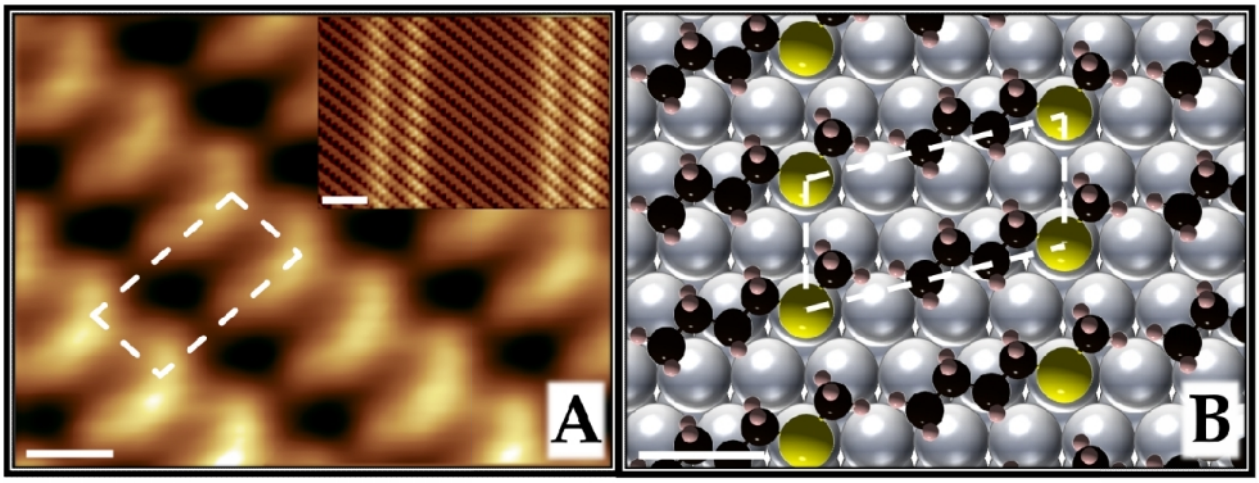

Figure 8. (A) STM image of a BMS domain at near-monolayer coverage on Au(111). Inset shows a larger scale image of the ordered domain, with the soliton walls appearing as vertical lines. (B) Schematic representation of the (√13 x √3) R13.9° unit cell. A & B scale bars indicate 0.5 nm; inset scale bar = 5 nm. Imaging conditions: I_t = *50 pA,* V_s = *100 mV, T = 80 K.*

A unique feature of clean Au(111) is its (22 x √3) or "herringbone" surface reconstruction, which results from 23 surface Au atoms being packed in a surface layer above 22 bulk atoms. This local compression along one of three close packed directions results in the emergence of stacking faults on the Au surface, in which fcc and hcp stacked atoms are separated by bright soliton walls, which protrude ~0.02 nm due to surface atoms sitting on top of bridge sites of the layer beneath. A pair of soliton walls comprises the "herringbone" and has a

highly regular periodic separation of 6.3 nm in native Au. In the presence of strongly interacting adsorbates, such as thioethers, phosphines or polyaromatic hydrocarbons, Au atoms are ejected from the surface layer, resulting in an elongation of the herringbone periodicity as the surface structure approaches that of un-reconstructed Au(111) 1x1.[32,39,53-56] This herringbone spacing can be used as a measure of adsorption strength.[39,53] Thiols adsorb strongly to the surface with ΔH_{ads} ≥ 130 kJ/mol and lift the herringbone reconstruction fully, yielding the (1 x 1) Au surface, while also removing additional Au atoms, resulting in the creation of etch pits.[30,42,57-61] However, the symmetric thioether DBS, ΔH_{ads} ~ 90 kJ/mol, only partially lifts the herringbone reconstruction.[42,62] We have previously shown with both BMS and DBS that the restructuring of the Au surface is an activated process and that annealing to ≥ 120 K is required in order for the Au surface restructuring to occur. Therefore, it is important to compare MTP with other systems that have been exposed to similar annealing temperatures.[39]

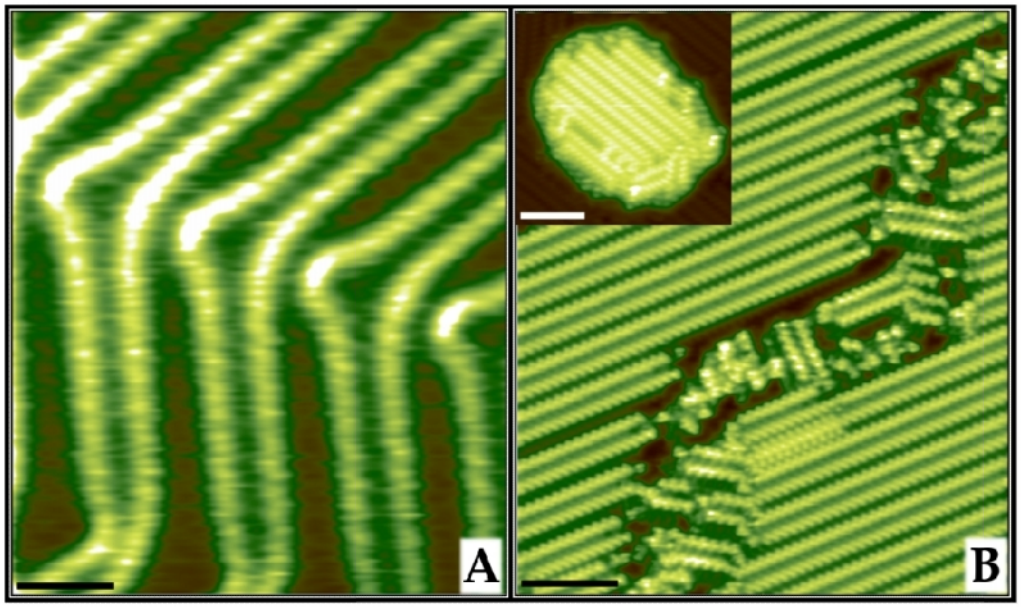

Figure 9. (A) STM image of clean Au(111) showing the regular array of solution walls that comprise the 22 x √3 or herringbone reconstruction with a repeating distance 6.3 nm. Imaging conditions: *I_t = 0.5 nA, V_s = -100 mV, T = 5 K.* (B) This image of identical size reveals that MTP adsorption at near-monolayer coverage lifts the herringbone

reconstruction as only one pair of soliton walls can be seen in a region with should contain four pairs. Inset displays a monolayer high Au island formed by Au atoms ejected by the herringbone reconstruction as it lifts. Imaging conditions: $I_t = 300\ pA$, $V_s = 100\ mV$, $T = 5\ K$. Scale bars indicate 5 nm.

After a 120 K anneal, BMS and DBS show herringbone spacings of 7.1 ± 0.3 nm and 7.6 ± 0.5 nm, respectively. MTP adsorption also lifts the herringbone reconstruction at this temperature as evidenced by widening of the soliton walls to 19.1 ± 0.7 nm (Figure 9B). The ejected Au atoms form islands on the terrace (Figure 9 inset) rather than diffusing to the lower-energy position at the step edges suggesting that Au atom ejection and MTP monolayer formation are both rapid and that the dense MTP overlayer prevents the migration of Au atoms. Thus we may rank the adsorption strength of these three compounds considering the degree to which the herringbone is lifted following a 120 K anneal: BMS ≈ DBS < MTP.

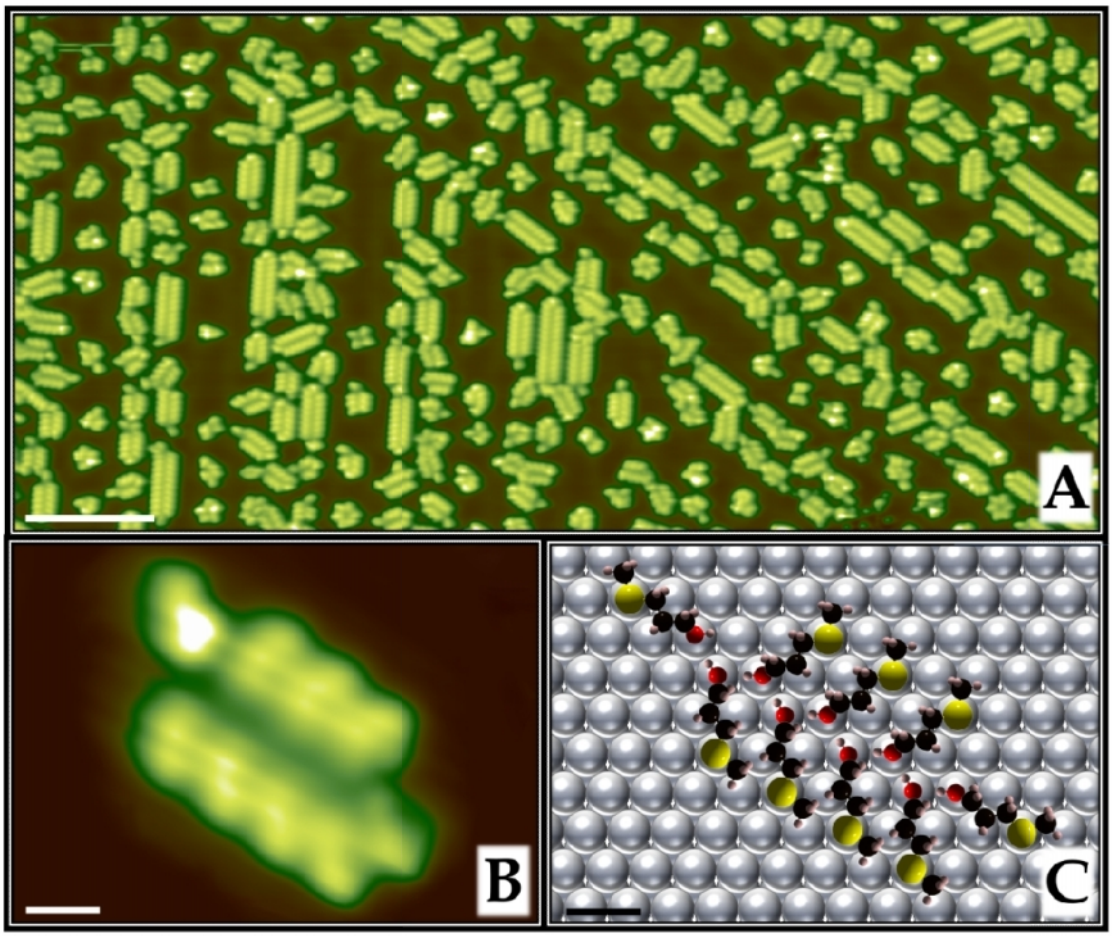

Figure 10. (A) MTP after 300 K anneal—coverage of ~0.5 ML. Scale bar = 10 nm. Imaging conditions: I_t = *200 pA,* V_s = *-200 mV, T = 5 K.* (B) High resolution of a truncated chain. Imaging conditions: I_t = *250 pA,* V_s = *-100 mV, T = 5 K.* (C) Proposed model of truncated chain in B. Scale bars in B and C = 0.5 nm.

Upon annealing to room temperature, much of the MTP overlayer desorbed molecularly, substantiated by the lack of any surface-bound fragments. Desorption of MTP led to a partial return of the herringbone reconstruction (spacing = 9.5 ± 0.7 nm) and the formation of smaller MTP structures (Figure 10A). The larger of these structures are truncated chains (Figure 10B), while others are aggregates of six or fewer molecules, including high-symmetry, chiral hexamers (Figure 11A). This partial desorption is particularly interesting in contrast to the behavior of BMS and DBS since the desorption temperature can serve as a quantification of SAM stability.

A 300 K anneal is sufficient to completely desorb BMS, but barely perturbs the DBS overlayer, whereas MTP coverage is reduced by nearly half. Therefore, the DBS molecular overlayer is the most stable of the three, which infers that the van der Waals interactions in the two longer butyl tails confer a greater degree of stability than the additional OH group and O-Au interaction of the shorter-tailed MTP. Interestingly, MTP monolayers are more stable than those of BMS indicating that substituting a CH_3 group for a OH group in these identically sized molecules increases monolayer stability.

The thioether systems under review are fundamentally different in three ways. First and foremost, MTP is different from BMS and DBS by virtue of its OH moiety. This functional group directs the formation of chains with hydrogen bonded cores and, in doing so, directs the growth of stable 1D lamellar structures. This assembly behavior is in contrast to the large 2D domains of BMS and DBS, in which intermolecular interactions are dominated by van der Waals interactions. Secondly, DBS differs from BMS and MTP in the length of its alkyl tails—both being butyl groups, instead of butyl and methyl. Greater alkyl tail length enhances van der Waals interactions during packing, stabilizing the monolayer. Finally, DBS is a symmetric thioether, while BMS and MTP are prochiral in the gas phase and become chiral upon adsorption.[39,46] Of the two chiral adsorbates, only BMS forms homochiral domains as seen in Figure 8.[39] We propose that MTP chains, both at monolayer and submonolayer coverage, are heterochiral at the surface-bound O atom. This O atom in the adsorbed state is surrounded by a H atom, a CH_2 group, a Au atom and a lone electron pair in a roughly tetrahedral arrangement and hence is chiral. Heterochiral chains allow for the OH-trimethylene backbone bond angle to remain relatively constant on both sides of the chain, as shown in Figure 5B. Further evidence for MTP chains being heterochiral is found in the smaller aggregates of MTP shown in Figure 10, which

again are equilibrium structures present after 300 K anneal. Their central hydrogen bonded network requires MTP molecules on either side of the chain to have surface bound O atoms of opposite chirality. While the S atom in surface-bound MTP is also chiral, the orientation of the methyl group is hard to measure with certainty; therefore, without assignment of chirality at both chiral centers, we are unable to discuss the MTP overlayer arrangement in terms of diastereomeric interactions.

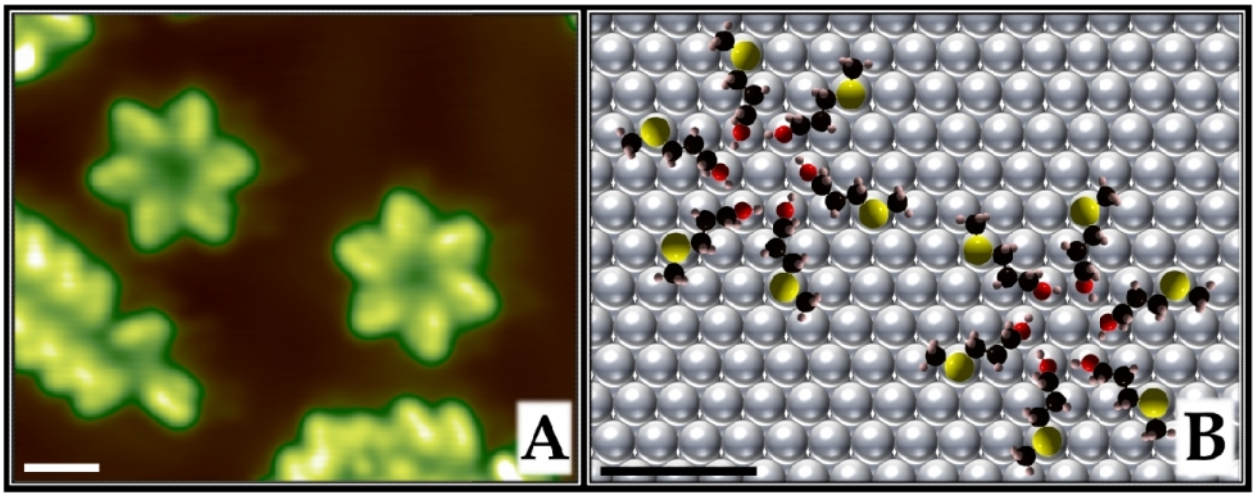

Figure 11. (A) Two MTP hexamers of opposite chirality on Au(111). (B) Schematic representations of each hexamer, with inverted chirality and the hydrogen bonded networks running in opposite directions. Scale bars = 1 nm. Imaging conditions: $I_t = 250\ pA$, $V_s = 200\ mV$, $T = 5\ K$.

The most common motifs present after a 300 K anneal resemble the chains present at high coverage but are of shorter length (Figure 10). Figure 10C shows a schematic of the proposed molecular arrangement in such truncated chains, wherein each of the two terminal molecules has only one hydrogen bond, as opposed to the interior molecules that each has two. Note that in Figure 10B the upper-left molecule in the chain appears brighter than the rest which is indicative of a dangling OH bond.[63-65] Nearly all truncated chains show a "capping" effect in

that they do not terminate with the same structure as the chain interior but have one or two extra molecules at each end in fewer symmetric positions. As the truncated chains are equilibrium structures, these molecules are presumably not kinetically trapped by the dangling hydrogen bonds but serve as more energetically favorable terminations that stabilize the chains.

The highest symmetry species of the low coverage aggregates are hexamers in which a cyclic network leaves every molecule with a full complement of two hydrogen bonds as seen in Figure 11. By analogy with methanol hexamers (Figure 6C), depending on the directionality of the hydrogen bonded network, two enantiomers of the hexamer structure appear as pinwheels slightly rotated with respect to one another and related by mirror symmetry. Interestingly, each chiral hexamer is composed of six surface-bound MTP enantiomers with surface bound O atoms of the same chirality and hence their assembly is enantiospecific. Thus, for both MTP and methanol, chirality is manifested by a unidirectional hydrogen bonded core centered about a single Au atom (Figure 6D and 11B). This motif gives further and perhaps the most conclusive evidence that the 1D chains are heterochiral. Six-molecule aggregates are present as both truncated chains and hexamers even though, in principle, if the chains were homochiral, a pinwheel-shaped hexamer would form upon truncation, as this maximizes hydrogen bonding.

Conclusions.

Hydrogen bonded networks are ubiquitous in nature and crucial for the integrity of many materials. The lipid bilayer, too, is a staple of life. Here we have shown that MTP spontaneously forms highly ordered structures on the Au(111) surface which resemble the lipid bilayer, and that hydrogen bonding plays a critical role in aligning the molecules to maximize both the hydroxyl network and intermolecular van der Waals interactions. Introduction of an OH group into the

thioether both directs and strengthens its molecular self-assembly on Au(111) as compared to the non-functionalized analogue. The resulting domains are based on lamellar structures with hydrogen bonded chains serving as backbones. The adsorption is strong enough to partially lift the Au surface's herringbone reconstruction but, unlike thiols, stops short of removing additional surface atoms. One especially intriguing aspect of these hydrogen bonded networks is that their structure implies that they must have directionality and, hence, an associated chirality. Comparing the chain and hexamer structures to a simpler molecule, methanol, allows us to assign relative chirality of the surface-bound OH group and reveal that the linear lamellar structures are heterochiral, whereas the cyclic hexamer structures are homochiral. This work demonstrates that introducing additional functionality into thioether monolayers is possible without sacrificing highly ordered domains and, in the case of terminal alcohols, can serve to direct the assemblies and stabilize the structures.

The molecule studied additionally constitutes an alternative surface-bound hydrogen storage system. Whereas methanol is a highly desirable hydrogen storage system due to its high hydrogen-to-carbon ratio for a given molecule, it desorbs from the gold surface at 155 K. Although MTP is over three-fold heavier than methanol, it is still present as a partial monolayer at room temperature. Thus, it represents a more robust avenue for surface-bound hydrogen storage.

Lastly, the chiral self-segregation of MTP molecules in hexamers at sub-monolayer coverage could be useful in the future as a vector towards enantioselective synthesis. These hexamers manifest the hydroxyl chirality of the molecules such that one could initiate a reaction local to a MTP hexamer of the desired chirality in order to favor a certain product.

Future Directions.

This work contributes significantly to the body of knowledge concerning thioether self-assembly and emphasizes the fact that a variety of unexplored functionalities exist in these systems with potentially exciting associated behaviors. With clever foresight, functionalized thioethers may be studied to address the shortcomings of thiols and leading eventually to the same degree of application that thiols have come to experience.

The work has furthermore demonstrated that multiple surface systems may converge without much technical synthetic work—MTP brings together the behaviors of BMS and methanol in a way that may be useful. It is worthwhile, then, to conceptualize other molecules which may stand at the crossroads of two or more interesting molecular overlayer systems, for it is at these crossroads that the optimal systems will likely be uncovered.

References.

(1) Binnig, G.; Rohrer, H. *IBM Journal of Research and Development* **1986**, *30*, 355.

(2) Binnig, G.; Rohrer, H. *Helv Phys Acta* **1982**, *55*, 726.

(3) Vitali, L.; Levita, G.; Ohmann, R.; Comisso, A.; De Vita, A.; Kern, K. *Nat Mater* **2010**, *9*, 320.

(4) Swart, I.; Sonnleitner, T.; Repp, J. *Nano Letters* **2011**, *11*, 1580.

(5) Repp, J.; Meyer, G.; Stojković, S. M.; Gourdon, A.; Joachim, C. *Phys Rev Lett* **2005**, *94*, 026803.

(6) Eigler, D. M.; Schweizer, E. K. *Nature* **1990**, *344*, 524.

(7) Crommie, M. F.; Lutz, C. P.; Eigler, D. M. *Science* **1993**, *262*, 218.

(8) Hla, S.-W.; Bartels, L.; Meyer, G.; Rieder, K.-H. *Phys Rev Lett* **2000**, *85*, 2777.

(9) Vickerman, J. C.; Gilmore, I. S. *Surface analysis : the principal techniques*; 2nd ed.; Wiley: Chichester, U.K., 2009.

(10) Guo, X.; Szoka, F. C. *Accounts of Chemical Research* **2003**, *36*, 335.

(11) Sackmann, E. *Science* **1996**, *271*, 43.

(12) Israelachvili, J. N.; Mitchell, D. J.; Ninham, B. W. *Biochimica et Biophysica Acta (BBA) - Biomembranes* **1977**, *470*, 185.

(13) Dameron, A. A.; Hampton, J. R.; Smith, R. K.; Mullen, T. J.; Gillmor, S. D.; Weiss, P. S. *Nano Lett.* **2005**, *5*, 1834.

(14) Donhauser, Z. J.; Mantooth, B. A.; Kelly, K. F.; Bumm, L. A.; Stapleton, J. J.; Price Jr, D. W.; Allara, D. L.; Tour, J. M.; Weiss, P. S. *Science* **2001**, *292*, 2303.

(15) Giancarlo, L. C.; Flynn, G. W. *Annual Review of Physical Chemistry* **1998**, *49*, 297.

(16) Giancarlo, L. C.; Flynn, G. W. *Accounts of Chemical Research* **2000**, *33*, 491.

(17) Love, J. C.; Estroff, L. A.; Kriebel, J. K.; Nuzzo, R. G.; Whitesides, G. M. *Chemical Reviews* **2005**, *105*, 1103.

(18) Poirier, G. E. *Chem. Rev.* **1997**, *97*, 1117.

(19) Poirier, G. E.; Tarlov, M. J. *Langmuir* **1994**, *10*, 2853.

(20) Poirier, G. E.; Tarlov, M. J.; Rushmeier, H. E. *Langmuir* **1994**, *10*, 3383.

(21) Smith, R. K.; Lewis, P. A.; Weiss, P. S. *Progress in Surface Science* **2004**, *75*, 1.

(22) Srinivasan, U.; Houston, M. R.; Howe, R. T.; Maboudian, R. *Journal of Microelectromechanical Systems* **1998**, *7*, 252.

(23) Stuart, D. A.; Yuen, J. M.; Lyandres, N. S. O.; Yonzon, C. R.; Glucksberg, M. R.; Walsh, J. T.; Van Duyne, R. P. *Analytical Chemistry* **2006**, *78*, 7211.

(24) Xia, Y. N.; Whitesides, G. M. *Annual Review of Materials Science* **1998**, *28*, 153.

(25) Qu, H. W.; Yao, W.; Garcia, T.; Zhang, J. D.; Sorokin, A. V.; Ducharme, S.; Dowben, P. A.; Fridkin, V. M. *Applied Physics Letters* **2003**, *82*, 4322.

(26) Hoertz, P. G.; Niskala, J. R.; Dai, P.; Black, H. T.; You, W. *Journal of the American Chemical Society* **2008**, *130*, 9763.

(27) Porter, M. D.; Bright, T. B.; Allara, D. L.; Chidsey, C. E. D. *Journal of the American Chemical Society* **1987**, *109*, 3559.

(28) Ford, J. F.; Vickers, T. J.; Mann, C. K.; Schlenoff, J. B. *Langmuir* **1996**, *12*, 1944.

(29) Kautz, N. A.; Kandel, S. A. *The Journal of Physical Chemistry C* **2012**, *116*, 4725.

(30) Kautz, N. A.; Kandel, S. A. *The Journal of Physical Chemistry C* **2009**, *113*, 19286.

(31) Noh, J.; Murase, T.; Nakajima, K.; Lee, H.; Hara, M. *The Journal of Physical Chemistry B* **2000**, *104*, 7411.

(32) Bellisario, D. O.; Jewell, A. D.; Tierney, H. L.; Baber, A. E.; Sykes, E. C. H. *The Journal of Physical Chemistry C* **2010**, *114*, 14583.

(33) Bain, C. D.; Biebuyck, H. A.; Whitesides, G. M. *Langmuir* **1989**, *5*, 723.

(34) Noh, J.; Jeong, Y.; Ito, E.; Hara, M. *Journal of Physical Chemistry C* **2007**, *111*, 2691.

(35) Noh, J.; Kato, H. S.; Kawai, M.; Hara, M. *Journal of Physical Chemistry B* **2002**, *106*, 13268.

(36) Noh, J.; Murase, T.; Nakajima, K.; Lee, H.; Hara, M. *Journal of Physical Chemistry B* **2000**, *104*, 7411.

(37) Troughton, E. B.; Bain, C. D.; Whitesides, G. M.; Nuzzo, R. G.; Allara, D. L.; Porter, M. D. *Langmuir* **1988**, *4*, 365.

(38) Weidner, T.; Kramer, A.; Bruhn, C.; Zharnikov, M.; Shaporenko, A.; Siemeling, U.; Trager, F. *Dalton Transactions* **2006**, *23*, 2767.

(39) Jewell, A.; Tierney, H.; Zenasni, O.; Lee, T.; Sykes, E. *Topics in Catalysis* **2011**, *54*, 1357.

(40) Jensen, S. C.; Baber, A. E.; Tierney, H. L.; H. Sykes, E. C. *ACS Nano* **2007**, *1*, 423.

(41) Jensen, S. C.; Baber, A. E.; Tierney, H. L.; Sykes, E. C. H. *ACS Nano* **2007**, *1*, 22.

(42) Lavrich, D. J.; Wetterer, S. M.; Bernasek, S. L.; Scoles, G. *The Journal of Physical Chemistry B* **1998**, *102*, 3456.

(43) Schönherr, H.; Kremer, F. J. B.; Kumar, S.; Rego, J. A.; Wolf, H.; Ringsdorf, H.; Jaschke, M.; Butt, H. J.; Bamberg, E. *Journal of the American Chemical Society* **1996**, *118*, 13051.

(44) Rojas, G.; Chen, X.; Kunkel, D.; Bode, M.; Enders, A. *Langmuir* **2011**, *27*, 14267.

(45) Tierney, H. L.; Calderon, C. E.; Baber, A. E.; Sykes, E. C. H.; Wang, F. *The Journal of Physical Chemistry C* **2010**, *114*, 3152.

(46) Tierney, H. L.; Han, J. W.; Jewell, A. D.; Iski, E. V.; Baber, A. E.; Sholl, D. S.; Sykes, E. C. H. *The Journal of Physical Chemistry C* **2010**, *115*, 897.

(47) x = 0.51615 nm with Gaussian 03W: Hartree Fock 6-31g

(48) Lawton, T. J.; Carrasco, J.; Baber, A. E.; Michaelides, A.; Sykes, E. C. H. *Physical Review Letters* **2011**, *107*, 256101.

(49) Baber, A. E.; Lawton, T. J.; Sykes, E. C. H. *The Journal of Physical Chemistry C* **2011**, *115*, 9157.

(50) Kashtanov, S.; Augustson, A.; Rubensson, J.-E.; Nordgren, J.; Ågren, H.; Guo, J.-H.; Luo, Y. *Physical Review B* **2005**, *71*, 104205.

(51) Zhang, H.-M.; Yan, J.-W.; Xie, Z.-X.; Mao, B.-W.; Xu, X. *Chemistry – A European Journal* **2006**, *12*, 4006.

(52) Gong, J.; Flaherty, D. W.; Ojifinni, R. A.; White, J. M.; Mullins, C. B. *The Journal of Physical Chemistry C* **2008**, *112*, 5501.

(53) Jewell, A. D.; Tierney, H. L.; Sykes, E. C. H. *Physical Review B* **2010**, *82*, 205401.

(54) Jewell, A. D.; Sykes, E. C. H.; Kyriakou, G. *ACS Nano* **2012**.

(55) Iski, E. V.; Jewell, A. D.; Tierney, H. L.; Kyriakou, G.; Sykes, E. C. H. *Surface Science* **2012**, *606*, 536.

(56) Iski, E. V.; Jewell, A. D.; Tierney, H. L.; Kyriakou, G.; Sykes, E. C. H. *Journal of Vacuum Science & Technology A: Vacuum, Surfaces, and Films* **2011**, *29*, 040601.

(57) Maksymovych, P.; Sorescu, D. C.; Dougherty, D.; Yates, J. T. *The Journal of Physical Chemistry B* **2005**, *109*, 22463.

(58) Maksymovych, P.; Sorescu, D. C.; Yates, J. T., Jr. *Physical Review Letters* **2006**, *97*, 146103.

(59) Rzeźnicka, I. I.; Lee, J.; Maksymovych, P.; Yates, J. T. *The Journal of Physical Chemistry B* **2005**, *109*, 15992.

(60) Nenchev, G.; Diaconescu, B.; Hagelberg, F.; Pohl, K. *Physical Review B* **2009**, *80*, 081401.

(61) Kautz, N. A.; Kandel, S. A. *Journal of the American Chemical Society* **2008**, *130*, 6908.

(62) Ruegg, M.; Jaques, R. *Experientia* **1972**, *28*, 1525.

(63) Hodgson, A.; Haq, S. *Surface Science Reports* **2009**, *64*, 381.

(64) Michaelides, A.; Morgenstern, K. *Nat Mater* **2007**, *6*, 597.

(65) Cerdá, J.; Michaelides, A.; Bocquet, M. L.; Feibelman, P. J.; Mitsui, T.; Rose, M.; Fomin, E.; Salmeron, M. *Physical Review Letters* **2004**, *93*, 116101.